Metal complexation and ion hydration in low density hydrothermal fluids: Ab initio molecular dynamics simulation of Cu(I) and Au(I) in chloride solutions (25–1000 °C, 1–5000 bar)

ARTICLE *in* GEOCHIMICA ET COSMOCHIMICA ACTA · APRIL 2014

Impact Factor: 4.33 · DOI: 10.1016/j.gca.2014.01.033

CITATIONS
14

READS
70

4 AUTHORS:

Yuan Mei
The Commonwealth Scientific and Industri…
28 PUBLICATIONS **96** CITATIONS
SEE PROFILE

Weihua Liu
Shanghai Jiao Tong University
52 PUBLICATIONS **690** CITATIONS
SEE PROFILE

David M. Sherman
University of Bristol
104 PUBLICATIONS **3,339** CITATIONS
SEE PROFILE

Joël Brugger
Monash University (Australia)
247 PUBLICATIONS **2,599** CITATIONS
SEE PROFILE

Available online at www.sciencedirect.com

ScienceDirect

Geochimica et Cosmochimica Acta 131 (2014) 196–212

Geochimica et Cosmochimica Acta

www.elsevier.com/locate/gca

Metal complexation and ion hydration in low density hydrothermal fluids: *Ab initio* molecular dynamics simulation of Cu(I) and Au(I) in chloride solutions (25–1000 °C, 1–5000 bar)

Yuan Mei [a,b], Weihua Liu [b], David M. Sherman [c], Joël Brugger [d,*]

[a] *Tectonics, Resources and Exploration (TRaX), School of Earth and Environmental Sciences, The University of Adelaide, Adelaide, SA 5005, Australia*

[b] *CSIRO Earth Science and Resource Engineering, Clayton, VIC 3168, Australia*

[c] *School of Earth Sciences, University of Bristol, Bristol BS8 1RJ, UK*

[d] *South Australian Museum, North Terrace, SA 5000, Australia*

Received 31 May 2013; accepted in revised form 27 January 2014; Available online 6 February 2014

Abstract

Low-density supercritical fluids are suspected of being able to transport metals, but it is unclear what the speciation/complexation would be in such conditions. In this work, we used *ab initio* molecular dynamics simulations to investigate the complexation, ion association and hydration of Cu^+ and Au^+ in NaCl brines as a function of solution density, from ambient to supercritical conditions (to 1000 °C, 5000 bar). Cu(I) and Au(I) form distorted linear complexes with two chloride ligands (i.e., $CuCl_2^-$ and $AuCl_2^-$) in subcritical chloride brines. We have discovered that these charged complexes remain in high density supercritical fluids even at high temperature; however, with decreasing density, these complexes become progressively neutralized by ion association with Na^+ to form low-charge $(Na_nCuCl_2)^{n-1}$ and $(Na_nAuCl_2)^{n-1}$ complexes. In these species, the Na^+ ion is very weakly bonded in the outer coordination sphere, resulting in highly disordered structures and fast (few picoseconds) exchange among coordinated and solvent Na^+ ions. Thermodynamic models to predict the solubility of metals in low-density magmatic or metamorphic fluids must account for these species. In addition, we found that the number of water molecules (i.e., the hydration number) surrounding the Cu^+, Au^+, Na^+ and Cl^- ions decreases linearly when fluid density decreases; this supports empirical thermodynamic models that correlate the stability constants of complexation reactions with solvent density. The traditional Born-model description explains the ion association as resulting from the decreased dielectric constant of the solvent. However at a molecular level, the increased ion association results from the increase in translational entropy associated with ion dehydration.

1. INTRODUCTION

In recent years there has been considerable speculation that low-density vapor phases may play a role in the transport of metals in magmatic hydrothermal ore deposits. A number of experiments have been carried out to investigate Cu(I) and Au(I) solubility in water vapor, and the partitioning of these cations between liquid/vapor/melt (e.g., Archibald et al., 2001, 2002; Pokrovski et al., 2005; Simon et al., 2005, 2006; Liu et al., 2008; Etschmann et al., 2010; Zajacz et al., 2010, 2011; Frank et al., 2011; Lerchbaumer and Audétat, 2012; Rempel et al., 2012). The solubilities

* Corresponding author. Current address: School of Geosciences, Monash University, Clayton, VIC 3800, Australia.

E-mail address: joel.brugger@monash.edu (J. Brugger).

http://dx.doi.org/10.1016/j.gca.2014.01.033

0016-7037/

of minerals in hydrothermal fluids is a consequence of the complexation of metals by ligands such as H_2O and Cl^-. Before we can model the dissolution, transport and deposition of metals from hydrothermal fluids, we need to know the identity, stoichiometry, and thermodynamic properties of aqueous metal complexes under wide ranges of temperature, pressure and fluid composition. The stoichiometry of metal complexes in aqueous solutions can be inferred from the dependence of mineral solubilities as a function of ligand concentrations. In water vapor, the fugacity of water (f_{H_2O}) appears to control metal transport and mineral solubility (Archibald et al., 2001, 2002; Williams-Jones et al., 2002), and this fugacity dependence has been used to infer hydration numbers of complexes. Archibald et al. (2001) conducted Au solubility experiments in subcritical, HCl-bearing water vapor at 300–360 °C and 144 bar, and suggested five (300 °C) and three (360 °C) water molecules around AuCl(g). A sister study of Cu(I) solubility (Archibald et al., 2002) found 7.6 and 6.1 waters around a Cu_3Cl_3(g) cluster at 320 and 280 °C, respectively. Liu et al. (2008) concluded that the solubility of nantokite (CuCl(s)) in supercritical water across the critical isochore (density of 0.19–0.42 g/cm^3) at 420 °C, 290–400 bar, is explained by a [H_2O–Cu–Cl](aq) complex with two extra water molecules in the second shell. Zezin et al. (2007, 2011) suggested $AuS(H_2O)_n$ in H_2S-water with $n = 2.3$ at 300 °C and 2.2 at 365 °C.

The assumption in these solubility models is that metal cations form neutral complexes in low-density fluids. This seems reasonable: as the fluid density decreases, the dielectric constant of the fluid decreases and we would expect charged complexes such as $CuCl_2^-$ to be unstable relative to neutral complexes such as CuCl(aq) or Cu_3Cl_3(aq). However, the speciation of Au and Cu may be more complicated than this picture: recently, Zajacz et al. (2010, 2011) discovered that the solubility of Au and Cu in magmatic volatile phases (1000 °C, 1500 bar) is strongly dependent upon the concentration of alkali cations (Na^+ or K^+); the presence of such cations increases metal solubility by up to an order of magnitude relative to that in systems where alkali cations were absent. Zajacz et al. (2010, 2011) hypothesized that, in high-temperature, low density fluids, Au(I) and Cu(I) are transported as neutral species due to the formation of outer-sphere complexes with alkali ions (e.g., neutral complexes $NaAuCl_2$(aq), $NaAu(HS)_2$(aq) and $NaCuCl_2$(aq)). Such complexes would also be expected to form as the dielectric constant of the solvent decreases.

It would be useful to directly identify changes in hydration number and outer-sphere ion-association in low-density fluids to confirm the interpretations of solubility experiments. Over the past 30 years, solubility experiments have been complemented by a growing number of *in situ* spectroscopic studies, in particular X-ray absorption spectroscopy (XAS), which enable us to directly identify metal species in solution over a wide range of conditions (reviews in Seward and Driesner, 2004; Brugger et al., 2010). Unfortunately, changes in hydration number and outer-sphere ion-association are very difficult to observe spectroscopically. *Ab initio* molecular dynamic simulations, however, provide a way to directly determine the nature of metal complexation. Previous examples include Zn(II)–Cl (Harris et al., 2003), Cu(I)–Cl (Sherman, 2007), Au(I)–HS (Liu et al., 2011), Ag(I)–Cl (Liu et al., 2012; Pokrovski et al., 2013), Cu–HS–Cl (Mei et al., 2013a), and Au(I)–HS/OH/S_3 (Mei et al., 2013b). These studies report outstanding agreement between the predicted nature and geometry of the complexes and available experimental studies. Mei et al. (2013a) also demonstrated that the formation free energies for important Cu(I) chloride and bisulfide complexes can be derived from *ab initio* MD simulations using thermodynamic integration; the complex formation stability constants compare well with the experimental ones, and, most importantly, enable accurate predictions of the mineral solubility gradients as a function of P, T and solution composition.

The goal of this work is to use *ab initio* molecular dynamics to determine the speciation of Au and Cu in low density fluids and test the hypothesis, suggested by solubility experiments, that changes in hydration and outer-sphere ion association enhance the solubility of Au and Cu in low density fluids. This case study provides an insight into the nature of neutral ion pairs and illustrates the stability of charged species up to high temperatures. The simulations also reveal an explanation for the empirical correlation between the stability constants of complexation reactions and solvent density (Dolejš and Manning, 2010; Dolejš, 2013).

2. METHOD: *AB INITIO* MOLECULAR DYNAMICS SIMULATIONS

2.1. Computational methods

Ab initio MD simulations of Cu(I) and Au(I) complexes at different densities (i.e., P, T conditions) were performed using the Car–Parrinello MD code "CPMD" (Car and Parrinello, 1985), which implements DFT using a plane-wave basis set and pseudo-potentials for the core electrons. The PBE exchange correlation-functional (Perdew et al., 1996) was employed with a cutoff of gradient correction 5×10^{-5}. Plane-wave cutoffs of 25 Ry (340.14 eV) were used together with Vanderbilt ultrasoft pseudo-potentials in CPMD package (Laasonen et al., 1993). A time-step of 3 a.u. (0.073 fs) was used to stabilize the simulations. The MD simulations were conducted in a NVT ensemble (i.e., constant composition, volume and temperature). Temperatures were controlled by Nosé thermostat for both the ions and electrons. Most simulations contained four Cl^-, one Au^+ or one Cu^+, and three Na^+ atoms to balance the charge in the solution. The pressures of the simulated systems were evaluated using the equation-of-state of NaCl solutions as implemented in the SOWAT code (Driesner, 2007; Driesner and Heinrich, 2007) based on a total equivalent NaCl salinity of 4 molal. To obtain time average of the geometric and stoichiometric information, radial distribution functions (RDF) and their integrals (related to coordination number) for different atom pairs were calculated by VMD (Humphrey et al., 1996).

Although the formal Cu or Au concentrations are one molal, the simulations represent dilute solutions with

respect to Cu or Au (no Cu–Cu or Au–Au interaction), because there is only one Cu or Au atom in each box. Most of the simulation systems listed in Tables 1 and 2 are undersaturated with respect to NaCl(s), except for some low-density fluids for which the NaCl concentrations exceed the solubility limit. For instance, the solubility of NaCl(s) reaches only 1.04 molal at 1000 °C, 1500 bar. In theory, the chloride concentration needs to be diluted by adding more water in the simulation box to represent the real fluid. But in practice, as discussed by Mei et al. (2013a), increasing the number of particles increases the simulation time dramatically, causing simulations to become prohibitively costly in terms of computing time. In this study, an *ab initio* MD simulation of the Cu–Cl system with 173 particles (55 H_2O, 1 Cu^+, 3 Na^+, 4 Cl^-, reflecting [Cl^-] of 4 molal) at a density of 0.29 g/cm^3 (box size 19.29 Å) required ~750 CPU hours per picosecond, while a simulation involving 341 particles (111 H_2O, 1 Cu^+, 3 Na^+, 4 Cl^-, reflecting [Cl^-] of 2 molal) cost more than 3500 CPU hours for one picosecond. The larger box also required longer time to reach steady state.

Two simulations at the same density (Cu–Cl system at the density of 0.29 g/cm^3) but with different numbers of water molecules (55 versus 111) were conducted to test the impact of box size on the results. The Cu–Na and Cl–Na pair distribution functions (Fig. 1a) show different intensities because in the simulation with the larger box, the Cu^+, Cl^- and Na^+ ions are diluted compared with the MD of the smaller box. However, the RDF integrals showing the number of Na^+ surrounding the Cu^+/Cl^- ions for both simulations overlap, indicating a small effect of the box size and dilution of the salt concentration from 4 to 2 molal. Similarly, the hydration numbers of Na^+ and Cl^- in the simulations with different box sizes agree well (Fig. 1b). Since the number of oxygen is about the same in a unit box (same solution density), the interactions of water with Cl^- and Na^+ are expected to be independent from the box size. The slight differences in the integrals of RDF result in calculated hydration number that are still very close (error <0.3) within a distance of 3.3 Å for Na–O and 3.8 Å for Cl–O (see Section 3.3 for choosing distance cutoff); these differences represent the magnitude of the uncertainty for the hydration number in our calculations, related mainly to the finite calculation time. Since the simulation of the smaller box is able to represent the features in the bigger box, we conducted simulations with 55 H_2O. To observe the behavior of the charge-balanced ions (Na^+) in the second-shell, long runs (> 20 ps) are necessary, since the atoms in the second-shell are more disordered than those in the first-shell.

Table 1
Simulation details and geometrical properties of Cu–Cl complexes in a box containing 1 Cu^+, 3 Na^+, 4 Cl^- and 55 H_2O. Time step is 3 a.u. (0.0726 fs). All the simulations were preformed for more than 29 picoseconds (400 000 steps).

Temperature (°C)	Pressure (bar)*	Box size (Å)	Density (g/cm^3)	Simulation time (ps)	Stoichiometry[a]	d_{Cu-Cl} (Å)	d_{Na-O} (Å)	d_{Cl-O} (Å)	Cl–Cu–Cl angle(°)
25	1	12.110	1.18	42.81	$[CuCl_3Na_{0.09}]^{-1.91}$	2.21	2.38	3.16	–
300	500	13.034	0.95	29.86	$[CuCl_2Na_{0.51}]^{-0.49}$	2.11	2.35	3.22	164.6(7.7)
300	1000	12.886	0.98	29.02	$[CuCl_2Na_{0.19}]^{-0.81}$	2.12	2.34	3.21	163.5(9.9)
300	2000	12.683	1.03	29.02	$[CuCl_2Na_{0.24}]^{-0.76}$	2.12	2.35	3.24	164.7(8.4)
500	600	14.658	0.67	29.02	$[CuCl_2Na_{0.45}]^{-0.55}$	2.12	2.35	3.26	160.3(11.7)
500	1000	14.030	0.76	29.02	$[CuCl_2Na_{0.48}]^{-0.52}$	2.12	2.34	3.26	161.2(10.1)
500	2000	13.434	0.87	29.86	$[CuCl_2Na_{0.32}]^{-0.68}$	2.11	2.35	3.24	161.1(11.3)
1000	1500	19.290	0.29	29.75	$[CuCl_2Na]^0$	2.11	2.35	3.32	153.6(14.9)
1000	2500	15.609	0.55	29.60	$[CuCl_2Na_{0.55}]^{-0.45}$	2.14	2.33	3.34	157.0(12.3)
1000	5000	14.128	0.74	34.32	$[CuCl_2Na_{0.59}]^{-0.41}$	2.13	2.33	3.31	157.1(13.7)

* Evaluated from the equation-of-state of NaCl fluids at the same ionic strength using the SOWAT code (Driesner, 2007; Driesner and Heinrich, 2007).
[a] Based on the number of Na atoms within 4.5 Å of a Cu atom.

Table 2
Simulation details and geometrical properties of Au–Cl complexes in a box with 1 Au^+, 3 Na^+, 4 Cl^- and 55 H_2O. Time step is 3 a.u. (0.0726 fs). All the simulations were preformed for more than 29 picoseconds (400 000 steps).

Temperature (°C)	Pressure (bar)*	Box size (Å)	Density (g/cm^3)	Simulation time (ps)	Stoichiometry[a]	d_{Au-Cl} (Å)	d_{Na-O} (Å)	d_{Cl-O} (Å)	Cl–Au–Cl angle(°)
300	500	13.034	1.05	32.65	$[AuCl_2Na_{0.42}]^{-0.58}$	2.28	2.35	3.25	169.5(5.4)
500	600	14.658	0.74	32.43	$[AuCl_2Na_{0.55}]^{-0.45}$	2.27	2.35	3.27	166.7(7.2)
500	2000	13.434	0.96	32.65	$[AuCl_2Na_{0.52}]^{-0.48}$	2.29	2.35	3.27	167.1(7.1)
1000	1500	19.290	0.32	31.93	$[AuCl_2Na_{0.89}]^{-0.11}$	2.32	2.34	3.32	159.2(10.7)
1000	2500	15.609	0.61	33.38	$[AuCl_2Na_{0.62}]^{-0.38}$	2.30	2.33	3.32	162.9(8.8)
1000	5000	14.128	0.82	32.65	$[AuCl_2Na_{0.67}]^{-0.33}$	2.30	2.34	3.32	163.8(9.6)

* Evaluated from the equation-of-state for NaCl fluids at the same ionic strength using the SOWAT code (Driesner, 2007; Driesner and Heinrich, 2007).
[a] Based on the number of Na atoms within 4.8 Å of a Au atom.

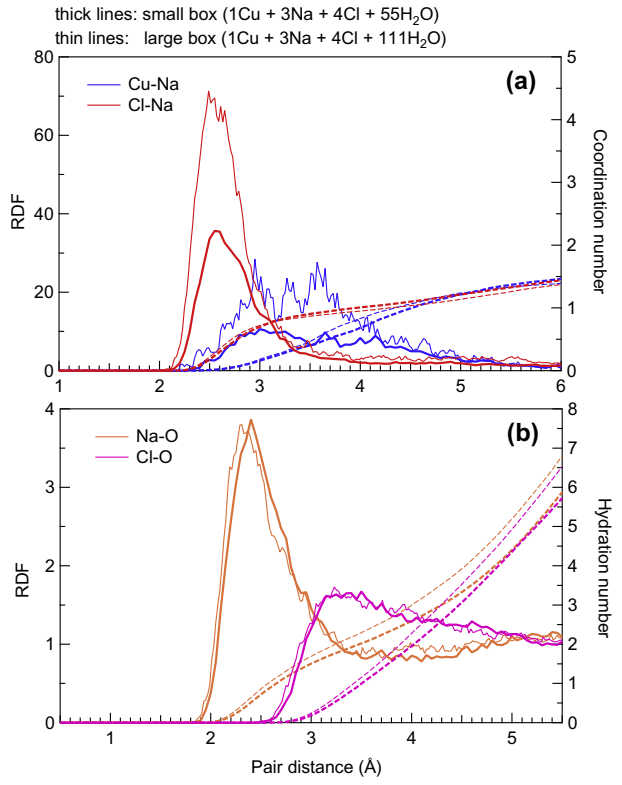

Fig. 1. Small box versus large box: the differences on RDF (left axes, solid curves) and coordination number (right axes, dashed curves).

2.2. Choice of model systems for comparison with experimental studies

In addition to the simulations aimed at exploring systematically the effect of solution density on the complexation and hydration of Au(I) and Cu(I) chlorocomplexes (Tables 1 and 2), five simulations were conducted at different T, P corresponding to specific experimental studies for direct comparison (Table 3). MD simulation of Cu(I) chloride complexes at a density of 0.29 g/cm^3 at 1000 °C, corresponding of a pressure of 1500 bar (No. 1) were performed to compare with the experimental study by Zajacz et al. (2011). Simulations No. 2 and 3 were conducted at 420 °C and pressures of 290 and 400 bar for comparison with the nantokite solubility, XANES and EXAFS data of Liu et al. (2008). The fluid densities shown in Table 3 are slightly higher than those listed by Liu et al. (2008), because the MD simulation were conducted at higher salt concentrations (1 molal Cu and 1 molal Cl) compared with real fluids. It is also notable that as the simulation box contained only one Cu and one Cl atoms, Cu–Cu and Cl–Cl interactions are negligible, reflecting the relatively dilute nature of the solutions studied by Liu et al. (2008). Simulation No. 4 was performed to compare with the experimental study by Archibald et al. (2001) of Au chloride solubility in water vapor (340 °C, 139 bar); a solution density of 0.10 g/cm^3 was chosen by using the pure water density of 0.082 g/cm^3 and adding one Au and Cl atoms to the simulation box (Table 3, No. 4). Simulation No. 5 was conducted to represent the liquid phase at the same temperature of 340 °C; the density was chosen at 0.79 g/cm^3 according to equation-of-state of NaCl fluids at the same ionic strength (Driesner, 2007; Driesner and Heinrich, 2007). All these simulations were conducted for more than 29 ps (400 000 simulation steps).

3. RESULTS

3.1. Cu(I) and Au(I) complexing as a function of solution density and temperature

MD simulation of Cu(I) in a 4 m Cl brine at 25 °C gave a threefold trigonal planar complex $CuCl_3^{2-}$ with the Cu–Cl distances of 2.21 Å (Table 1), in accordance with previous experimental (Brugger et al., 2007; Liu et al., 2008) and theoretical studies (Sherman, 2007; Mei et al., 2013a). At elevated T and P, twofold distorted linear complexes MCl_2^- (M = Cu/Au) were found in simulations of Cu–Cl and Au–Cl solutions, with Cu–Cl distances of 2.11–2.14 Å (Table 1) and Au–Cl distances of 2.27–2.32 Å (Table 2), in good agreement with previous experimental studies: Cu–Cl distance of 2.152(7) Å by Brugger et al. (2007) and 2.12–2.13 Å by Fulton et al. (2000a,b); Au–Cl distance of 2.27–2.28 Å by Pokrovski et al. (2009).

The configurations of MCl_2^- (M = Cu/Au) complexes with surrounding Na^+/Cl^- ions were investigated along

Table 3
Simulation details for runs aimed at comparing with experimental studies.

No.	Reference	Simulation box	T (°C)	P (bar)[a]	Box size (Å)	Density (g/cm^3)	Stoichiometry	$d_{Cu/Au-Cl}$ (Å)	$d_{Cu/Au-O}$ (Å)	Angle (°)
1	Zajacz et al. (2011)	1 Cu, 3 Na, 4 Cl, 55 H_2O	1000	1500	19.290	0.29	$[CuCl_2Na]^0$	2.11	–	155.4(13.4)
2	Liu et al. (2008)	1 Cu, 1 Cl, 55 H_2O	420	290	20.830	0.20	$CuCl(H_2O)^0$	2.09	1.93	164.1(8.6)
3	Liu et al. (2008)	1 Cu, 1 Cl, 55 H_2O	420	400	15.808	0.46	$CuCl(H_2O)^0$	2.10	1.94	163.1(8.8)
4	Archibald et al. (2001), vapor phase	1 Au, 1 Cl, 55 H_2O	340	139[§]	27.186	0.10[§]	$AuCl(H_2O)^0$	2.23	2.11	168.9(6.0)
5	Archibald et al. (2001), liquid phase	1 Au, 1 Cl, 55 H_2O	340	139	13.694	0.79	$AuCl(H_2O)^0$	2.24	2.08	168.9(6.1)

[a] Pressures evaluated from equation-of-state of NaCl fluids at the same ionic strength using the SOWAT code (Driesner, 2007; Driesner and Heinrich, 2007).
[§] Evaluated from the equation-of-state of the vapor phase using the pure water density of 0.082 g/cm^3; the density of the AuCl solution is 0.10 g/cm^3.

the simulation time at different P, T conditions to test if and how the MCl_2^- complexes form neutral species as a function of fluid density and temperature. The results show that charged species (i.e., MCl_2^-) predominate in high-density fluids (>0.7 g/cm^3), even in high-temperature supercritical fluids. In low density fluids, however, the probability of forming the neutral species $MNaCl_2(aq)$ and larger clusters such as $MNa_nCl_m^{1+n-m}$ increases. Selected snapshots of the Cu–Cl simulation at 1000 °C, 1500 bar (density 0.29 g/cm^3, No. 1 in Table 3) reveal that the neutral $CuNaCl_2(aq)$ species does not display a well-characterized geometry (e.g., configurations at 10.97 and 15.8 ps; Fig. 2a and b). The simulation also occasionally shows charged species and larger clusters; for example at 24.5 ps (Fig. 2c and d), the $CuCl_2^-$ cluster is weakly linked to a NaCl(aq) cluster. Over the next 0.7 ps, this cluster evolves into a $CuNa_2Cl_3(aq)$ cluster (Fig. 2d–g). A similar situation is found for the Na^+ ions in this solution; the neutral cluster NaCl(aq) is present at 10.97 ps (Fig. 2a), but at 15.8 ps the $Na_2Cl_2(aq)$ cluster formed (Fig. 2b). At 24.5 ps, the simulation contains a Na_2Cl^+ cluster in addition to a $NaCuCl_2(aq)$ cluster.

The dynamic distances between the Cu and Na atoms as a function of simulation time also indicate the extent of Na^+ pairing with $CuCl_2^-$. The evolutions of Cu–Na distances and instantaneous coordination numbers for three simulations at three different T, P conditions, with fluid densities ranging from 0.29 to 1.03 g/cm^3, are shown in Fig. 3. At a density of 0.29 g/cm^3 (1000 °C, 1500 bar; Fig. 3a and b), there is at least one Na^+ ion at a distance of ~3–5 Å from Cu^+. The closest Na^+ ions exchange at a very fast rate (longest residence time <15 ps), compared with the exchange rates of H_2O and Cl^- in aqua- and chloride complexes of transitions metals, which lie in the ns to μs range (Table 11.4 in Burgess, 1978; Sharps et al., 1993). For short periods (<3 ps), two or three Na^+ ions get close to Cu^+, forming large clusters (e.g., Fig. 2g). The running average of instantaneous coordination number gave an average number of one Na^+ surrounding Cu^+ (within 4.5 Å). In contrast, at the density of 0.67 g/cm^3 (Fig. 3c and d), Cu^+ and Na^+ only bind together occasionally, with an average of 0.45 Na^+ within 4.5 Å of Cu^+. In the simulation at 300 °C, 2000 bar (Fig. 3e and f), with a density of 1.03 g/cm^3, there is less chance for Na^+ to complex to Cu^+, which is also confirmed by the instantaneous coordination number (0 is predominant, as shown in Fig. 3f).

Fig. 4a shows the Cu–Na RDF at different temperatures and densities (solid lines), together with the integrals of the selected distribution functions, representing the number of Na^+ surrounding Cu^+ ($N_{Na(Cu)}$) (dashed lines). There is a clear trend that the height of the RDF peak and $N_{Na(Cu)}$ decrease with increasing density. At a density of 0.29 g/cm^3 (1000 °C, 1500 bar), there is a large peak between 2.5 and 4.5 Å, and $N_{Na(Cu)}$ is one at the distance of 4.5 Å. This shows the predominance of the neutral species (e.g., $CuNaCl_2(aq)$), although the width of the RDF shows that Na^+ is only weakly bond. The distribution functions of Cu–Na agree with the distance plots shown in Fig. 3,

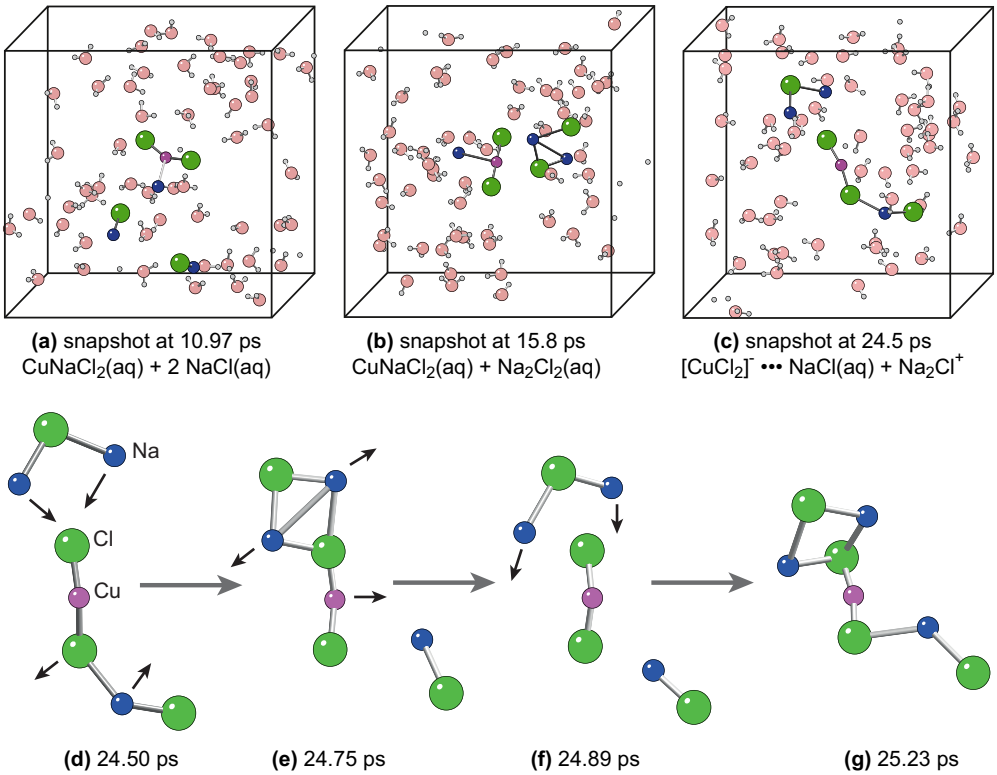

Fig. 2. Cu^+ and Na^+ local structures at 1000 °C, 1500 bar (0.29 g/cm^3). (a–c) Selected snapshots of simulations. (d–g) Example of dynamic transformation of Cu(I) ion pairs.

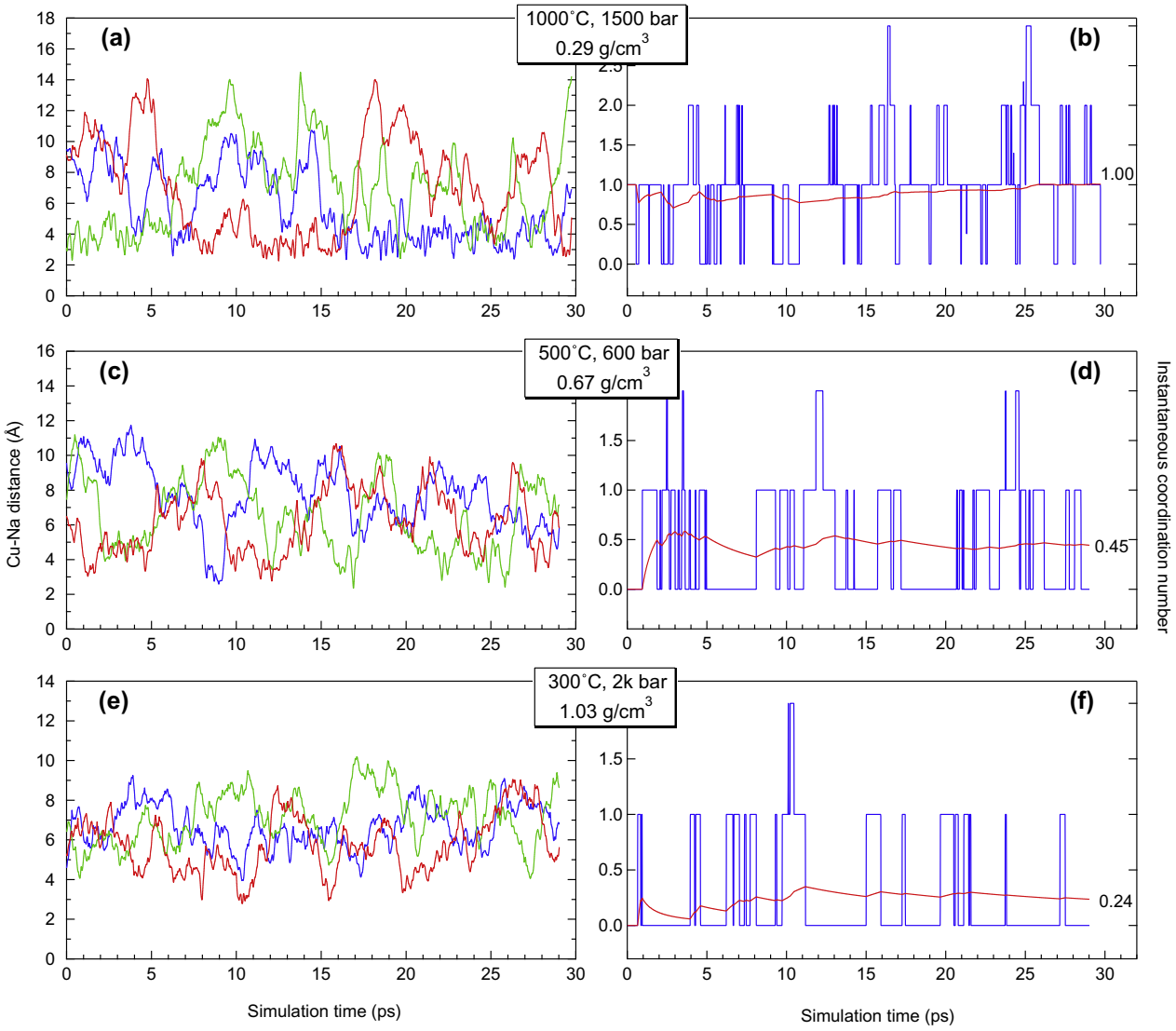

Fig. 3. Cu–Na distance versus simulation time (left) and instantaneous coordination number (distance cutoff = 4.5 Å) together with running average as a red line (right). (For interpretation of the references to colour in this figure legend, the reader is referred to the web version of this article.)

indicating there are more neutral complexes in low-density fluids and more charged complexes in high-density fluids.

For Au^+, the Au–Na RDF and their integral indicate that an analogous neutral species, $NaAuCl_2$(aq), predominates at low density (0.32 g/cm^3), with an average of 0.89 Na^+ within 4.8 Å of Au^+ (Table 2). The number of Na^+ surrounding Au^+ decreases to 0.42 with an increase of density to 1.05 g/cm^3. Fig. 5a shows the RDF (solid lines) and coordination number (dashed lines) of Au–Na at different temperatures and densities. Similar to what was observed for the Cu–Cl systems, the RDF peak intensity and the numbers of Na surrounding Au decrease with increasing density (Fig. 5a). At the density of 0.32 g/cm^3 (1000 °C, 1500 bar), the RDF peak at 2.8–4.8 Å (Fig. 5a) indicates the predominance of the neutral $AuNaCl_2$(aq) species with weakly bond Na.

In addition to the neutral $MNaCl_2$(aq) (M = Cu,Au) complexes, the MD simulations also show that Na^+ and Cl^- form a number of neutral ion pairs in low-density fluids (e.g., Fig. 2a and b). Since there are 3 Na^+ and 4 Cl^- in the simulation box, it would be difficult to show each Cl–Na distances. Here we calculated the RDF of Cl–Na pairs and the number of Na^+ surrounding Cl^- ($N_{Na(Cl)}$). The RDF peaks of the Cl–Na pairs decrease with an increase in density, and $N_{Na(Cl)}$ decreases, too (Figs. 4b and 5b). At 1000 °C, 1500 bar, $N_{Na(Cl)}$ is ~1, corresponding to the NaCl(aq) species shown in Fig. 2a. In contrast, the Cl–Na RDF peak is very weak at room temperature, consistent with the predominance of the Na^+ and Cl^- aqua ions. The classical MD simulations of NaCl solutions of Driesner et al. (1998) showed that aqua ions account for 63.3% Na or Cl at room temperature (density of 1.02 g/cm^3). At 380 °C (density of 0.55 g/cm^3) this proportion decreases to 12.8%; neutral ion pairs ($NaCl^0$, $Na_2Cl_2^0$, $Na_3Cl_3^0$, $Na_4Cl_4^0$) contribute 49.8% and charged clusters (Na_2Cl^+, $NaCl_2^-$, $Na_3Cl_2^+$, $Na_2Cl_3^-$, $Na_4Cl_3^+$, $Na_3Cl_4^-$) contribute

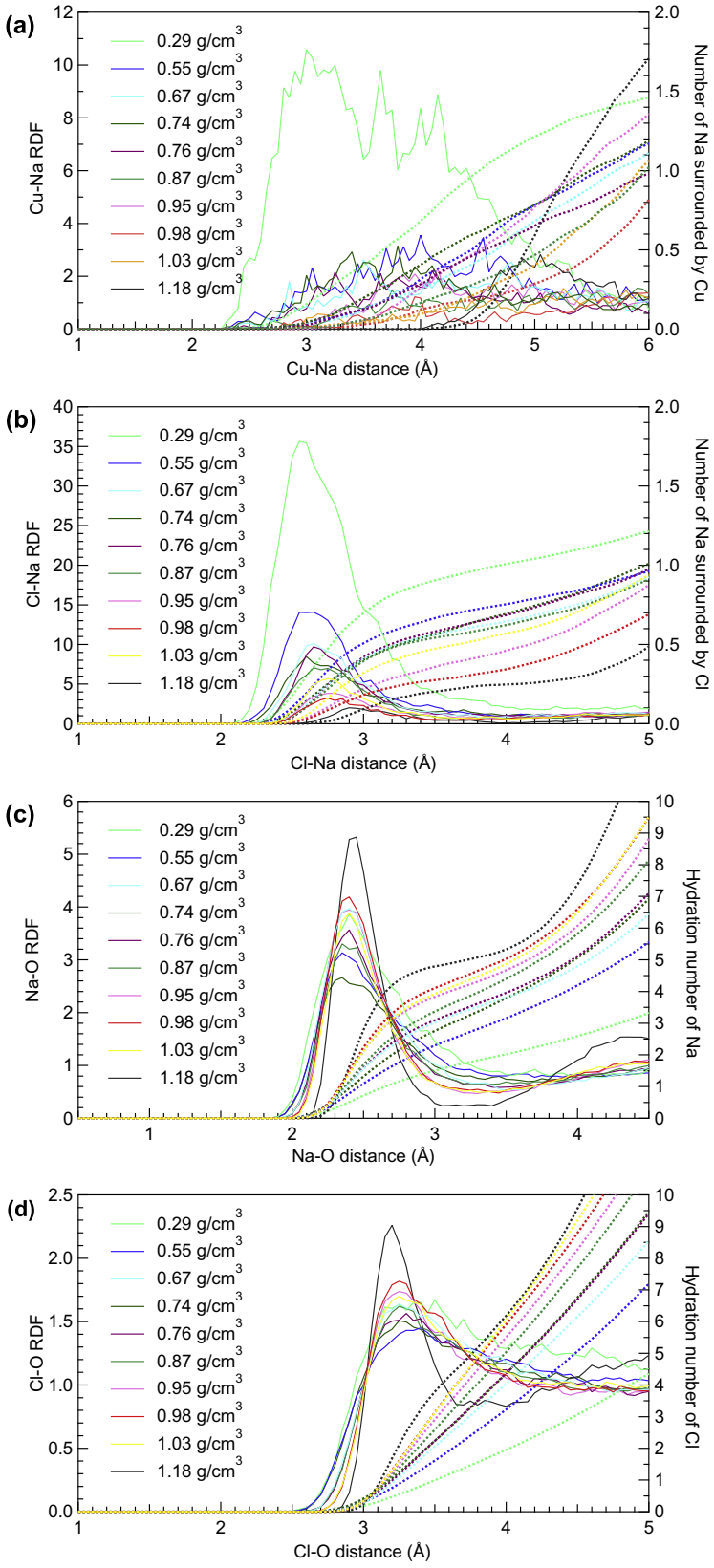

Fig. 4. Radial distribution functions and the integrals of Cu–Na, Cl–Na, Na–O, Cl–O pairs at different solution densities (see Table 1 for temperatures and pressures).

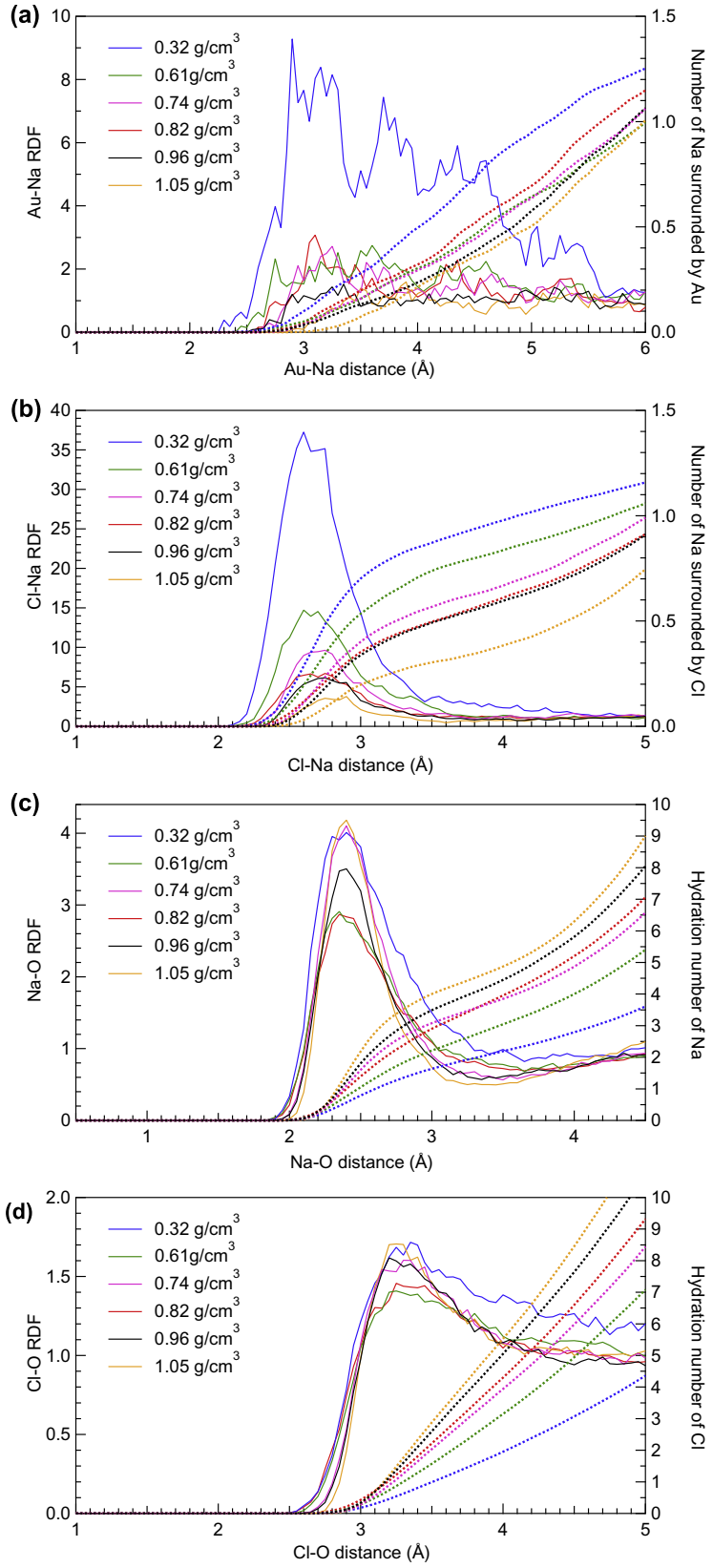

Fig. 5. Radial distribution functions and the integrals of Au–Na, Cl–Na, Na–O, Cl–O pairs at different solution densities (see Table 2 for temperatures and pressures).

37.4% to total solute species. Hence, our *ab initio* calculations confirm the results of earlier classical calculations in emphasizing the importance of the neutral NaCl(aq) species, together with short-lived, larger clusters for understanding the properties of high temperature brines (Driesner et al., 1998).

To further illustrate the relationship between fluid density and the number of Na^+ surrounding Cu(I) and Au(I) complexes ($N_{Na(Cu)}$, $N_{Na(Au)}$), as well as Na–Cl ion pairing ($N_{Na(Cl)}$), quantitative values of $N_{Na(X)}$ were obtained from RDF plots. One challenge in defining $N_{Na(X)}$ is to choose an appropriate distance cutoff. The distance cutoff is usually set at the shoulder of the integral of the RDF plot, and can vary slightly with temperature (e.g., Driesner et al., 1998). In this study, we chose to fix the distance cutoff for all temperatures, to avoid bias in the temperature trends. A cutoff distance at 3.4 Å was set for the Cl–Na pair according to Fig. 4b at the end of the Cl–Na RDF peak. For the Cu–Na and Au–Na distribution functions, the RDF peak is not very sharp and the data are affected by significant noise, making it difficult to define the cutoff distance. Yet we need to find a safe cutoff distance that includes the possible bonding Cu–Na and Au–Na pairs but excludes the random Na movement and the impact of different box size. As shown in Fig. 4a, the RDF peak appears at ~2.5–4.5 Å for low densities and ~3–4.5 Å for high densities. A cutoff distance of 4.5 Å was chosen to calculate $N_{Na(Cu)}$. Using this value, a fully neutral ion pair ($N_{Na(Cu)} = 1$) is predicted at 1000 °C, 1500 bar, consistent with the results of Zajacz et al. (2011). A cutoff distance of 4.8 Å was set for calculating $N_{Na(Au)}$, as static calculations indicate a Au–Na distance about 0.3 Å longer than Cu–Na (Zajacz et al., 2011), which is also apparent in the MD results statistically (Fig. 5a). The uncertainties of ion pairing were evaluated by calculating the standard deviation among fragments of $N_{Na(Cu)}$ over the time period of 5 ps. Plots of number of Na^+ surrounding Cu^+ or Au^+ as a function of density (Fig. 6a) show a good linear relationships, with correlation coefficients (R^2) of 0.92 for $N_{Na(Cu)}$ and 0.84 for $N_{Na(Au)}$. Excellent linear correlations also hold for Cl, with correlation coefficients between density versus $N_{Na(Cl)}$ of 0.87 for Cu-MD and 0.92 for Au-MD (Fig. 6b). All these linear fitting of density versus ion pairing took the uncertainties into account. As the density of NaCl–H_2O fluids is well constrained (e.g., equation-of-states by Driesner, 2007; Driesner and Heinrich, 2007), the correlations versus solution density for Au were similar with the dielectric constant of pure water ($R^2 = 0.86$), but significantly better for Cu ($R^2 = 0.40$) than the correlation with the dielectric constant of pure water (Fig. S1).

3.2. Hydration numbers of Na, Cl, Cu and Au

To calculate the hydration of Na^+ and Cl^-, distances of 3.3 and 3.8 Å, respectively, were chosen according to the RDF plot (Fig. 4c and d, Fig. 5c and d). Similarly, a cutoff distance of 5.0 Å was chosen to calculate the hydration numbers of Cu^+ and Au^+. The calculated hydration numbers together with the uncertainties evaluated using the method mentioned before are plotted as a function of solution density in Fig. 6(c and d). The number of water molecules surrounding Na ($Hyd_{(Na)}$) and Cl ($Hyd_{(Cl)}$) increases with increasing solution density (Figs. 4c and d and 6c for Cu-MD; Figs. 5c and d and 6d for Au-MD). For example,

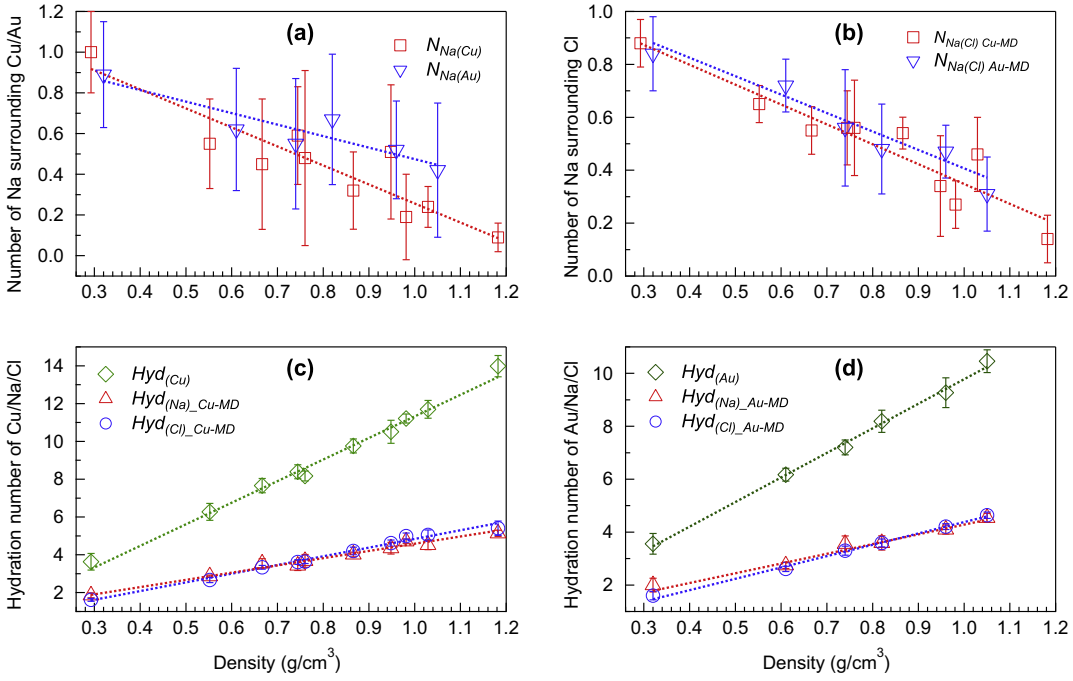

Fig. 6. The number of Na surrounding Cu/Au (a) and Cl (b), and the hydration number of Na/Cl/Cu (c) and Na/Cl/Au (d) as function of solution density.

there are ~5 waters surrounding Na at a density of 1.18 g/cm^3, but the number decreases to ~2 at a density of 0.29 g/cm^3 (Figs. 4c and 6c). The hydration numbers of Na^+ and Cl^- in Au–Cl solutions gave similar results (Figs. 5c and 6d). Good linear correlations between the hydration number of Na^+, Cl^-, Cu^+ and density were obtained. For Cu–Cl fluids, linear correlation coefficients R^2 of 0.98, 0.99 and 0.99 for $Hyd_{(Na)}$, $Hyd_{(Cl)}$ and $Hyd_{(Cu)}$ were obtained (Fig. 6c); and Au–Cl solutions gave R^2 of 0.98, 0.99 and 0.99 for $Hyd_{(Na)}$, $Hyd_{(Cl)}$ and $Hyd_{(Au)}$, respectively (Fig. 6d).

The simulations of 1 Cu, 1 Cl and 55 H_2O at temperature of 420 °C and densities of 0.20 and 0.46 g/cm^3 (No. 2 and 3 in Table 3) gave the predominant complex $CuCl(H_2O)$(aq), consistent with the interpretation of the experiments by Liu et al. (2008). In the calculation of the hydration number of Cu^+ and Cl^-, the first shell water in the linear $CuCl(H_2O)$(aq) complex was excluded. The hydration numbers of Cu^+ and Cl^- both increase with increasing density (Fig. 7). Specifically, there are 4.26 water molecule within the distance of 5.0 Å of Cu^+ at a density of 0.20 g/cm^3 (400 °C, 290 bar, vapor-like fluids); this hydration number increases by ~3 (6.95 water molecules) at a density of 0.46 g/cm^3 (400 °C, 400 bar). The hydration number of Cl^- increased from 1.28 (0.20 g/cm^3) to 1.97 (0.46 g/cm^3).

The simulation of Au–Cl in both vapor and liquid phases (No. 4 and 5 in Table 3) gave a predominant species of $AuCl(H_2O)$(aq). Fig. 8 shows the instantaneous hydration numbers of Au^+ and Cl^-, excluding the first shell water in the $AuCl(H_2O)$(aq) complex. In simulation No. 5, which represents the $AuCl(H_2O)$(aq) complex in a liquid phase with a density of 0.79 g/cm^3, MD gave a hydration number of nine for the second-shell (Fig. 8a). In contrast, in a vapor phase (equivalent pure water density of 0.082 g/cm^3; AuCl fluid density of 0.10 g/cm^3) at identical P, T, simulation No. 4 gave a hydration number of three in the second-shell (Fig. 8c), i.e., a total hydration number of four. The hydration of chloride also decreased dramatically from liquid to vapor phase (from 2.73 to 0.71, Fig. 8b and d). Based on measurements of Au(s) solubility in HCl-bearing steam, Archibald et al. (2001) concluded that the total hydration number for the Au(I) complex decreased from 5 to 3 as temperature increased from 300 to 360 °C at constant pressure, agreeing with our conclusion that the hydration of Cu/Au complexes decreased with decreasing density (since at the same pressure, density decreases with increasing temperature). Archibald et al. (2001) obtained a total hydration number of four at 340 °C, as same as we calculated from the MD simulations.

3.3. Na–O and Cl–O bond distances

Whereas the hydration numbers of the Na^+ and Cl^- ions are correlated with solution density, the Na–O and Cl–O bond distances are correlated with temperature. The Na–O distances decrease from 2.38 Å at 25 °C to ~2.33 Å at 1000 °C (Tables 1 and 2). On the other hand, Cl–O distances increase from 3.16 Å at 25 °C to ~3.32 Å at 1000 °C. The same trends were discovered by Driesner et al. (1998) by classical MD simulations, in which Na–O distances decreased by 0.03 Å (from 2.26 to 2.23 Å) and Cl–O distances increased by 0.02 Å (from 3.22 to 3.24 Å) over a temperature increase from 27 to 317 °C.

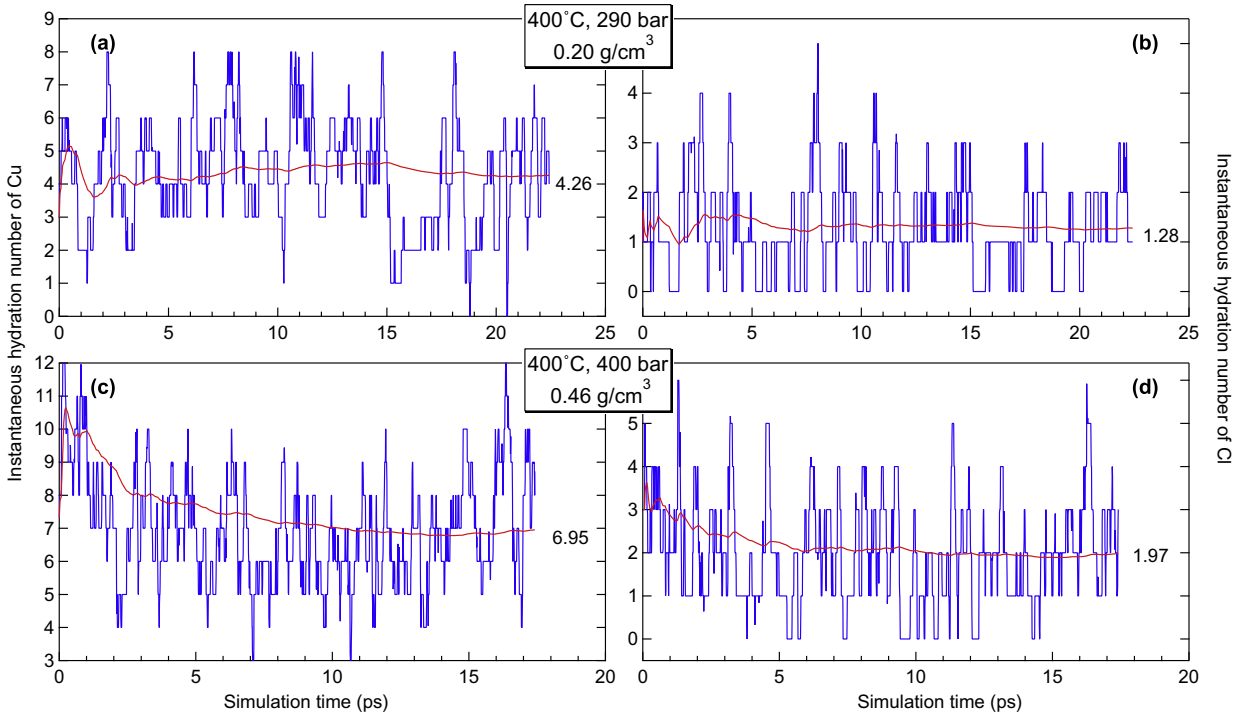

Fig. 7. Instantaneous hydration numbers of Cu (a and c) and Cl at different T, P conditions (b and d) (without the first shell water).

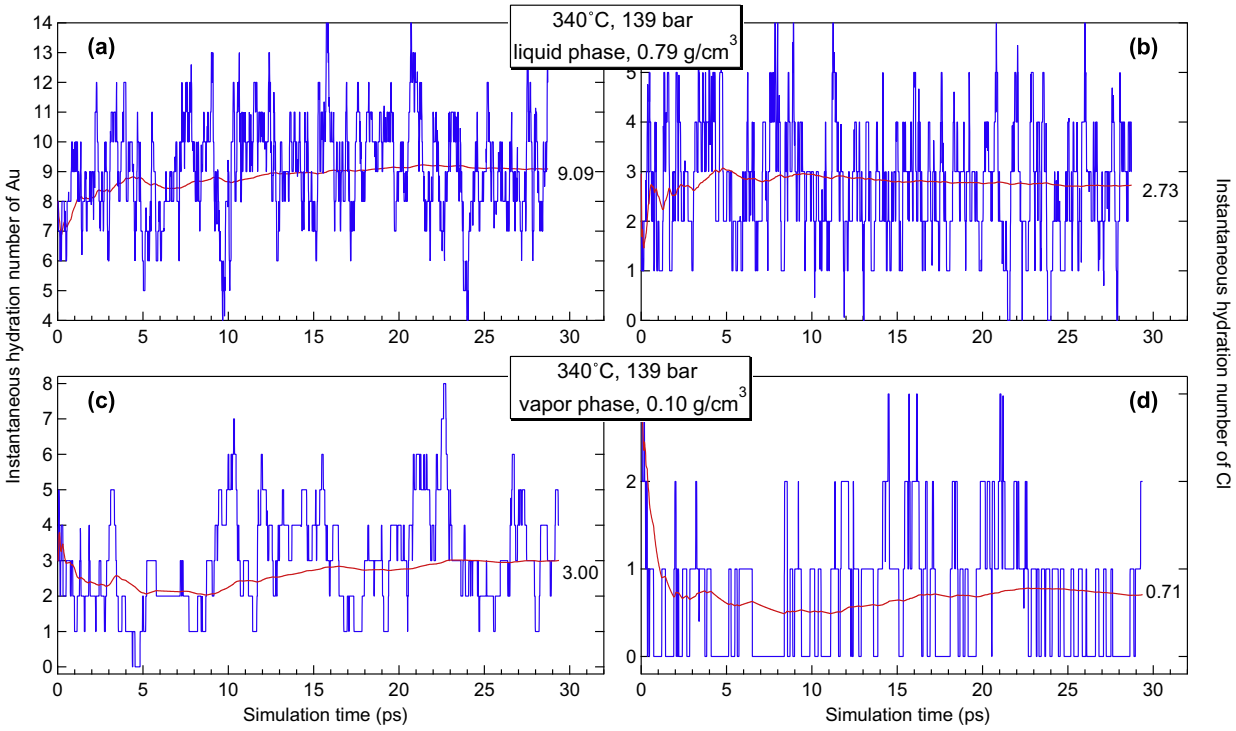

Fig. 8. Instantaneous hydration numbers of Au (a and c) and Cl (b and d) in coexisting liquid phase and vapor phases at 340 °C (without the first shell water).

4. DISCUSSION

4.1. The nature of neutral Cu(I) and Au(I) chloro-complexes

Zajacz et al. (2010, 2011) have demonstrated experimentally that the solubility of Cu and Au in low density, high temperature supercritical fluids (1000 °C, 1500 bar, 0.29 g/cm^3) is dependent upon the nature and concentration of alkali ions, a fact that can be explained by the formation of neutral species such as $MCl_2Na(aq)$ (M = Au,Cu). Zajacz et al. (2011) also report static quantum chemical calculations for linear Cu(I) chloride and bisulfide complexes, suggesting that the $NaCuCl_2(aq)$ and NaCuClHS(aq) species are inner sphere complexes. These calculations are performed for selected complex stoichiometries, and relate to the ideal gas phase, or use a "Polarizable Continuum Model" to represent the solvent, which is characterized by its dielectric constant (Cossi et al., 1996). In the optimized structures from the static calculations and during most of the MD simulations, Na occurs sideways from the center Cu atom of the linear $CuCl_2^-$ moiety in the $CuNaCl_2(aq)$ cluster (Fig. 2a and b), with Cu–Na distances of 2.73 Å from the static calculations versus ~3.0–4.0 Å by MD (Fig. 4a).

The static calculations, however, cannot predict the disorder and residence time of this configuration, or the fact that different geometries appear with a statistically significant likelihood. The picture arising from our *ab initio* MD simulations provided more details:

i) Explicit inclusion of the water molecules in MD simulations results in $CuCl_2^-$ having a distorted linear geometry, consistent with the experimental measurements, even in the absence of Na^+ within the first or second coordination shells (see also Mei et al., 2013a). This shows that hydration has a large effect on the complex geometry, so that MD simulations with explicit water molecules provide a better prediction of the structures than the static calculations based on isotropic continuum solvent models.

ii) Although the MD simulations show the predominance of a neutral $MCl_2Na(aq)$ ion pair in low density, high temperature solutions at conditions similar to the experiments of Zajacz et al. (2010, 2011), the nature of the complex differs fundamentally from the picture suggested by static quantum mechanical calculations. The Na^+ ion is only weakly bonded (weak electrostatic bonding), as shown by the large range in M–Na distances, the lack of definite coordination geometry for the neutral ion pair, and extremely fast exchange rate of the bonded Na^+ (<15 ps) (Figs. 2 and 3). These exchange rates are fast relative for example to the H_2O residence times for divalent aqua-ions, with range from 0.2 ns for Cu^{2+} to 30 μs for Ni^{2+} (Table 11.4 in Burgess, 1978). Therefore we suggest that Na^+ is loosely bounded in the outer coordination sphere. The MD simulations also demonstrate that atoms bounded at the

outer sphere (or second shell) are unlikely to be detected by EXAFS studies (e.g., Fulton et al., 2000a,b; Liu et al., 2001, 2008; Brugger et al., 2007 for Cu), because of the wide spread in Cu–Na bond distances (i.e., large Debye–Waller factor).

4.2. Density dependence of the charged or neutral complexes

When dealing with metal speciation in hydrothermal fluids, one of the fundamental assumptions is that in supercritical fluids, neutral species will predominate over charged species, because of a dramatic decrease in the dielectric constant of water with increasing temperature (Barnes, 1997). Our *ab initio* MD simulations accurately reproduce the expected trend towards a predominance of neutral clusters over charged complexes with decreasing fluid density and dielectric constant. This trend has been demonstrated before for NaCl brines on the basis of classical MD studies (e.g., Driesner et al., 1998; Sherman and Collings, 2002), showing an increase in the stability of large clusters in supercritical fluids. For example, the Na_2Cl_2(aq) cluster is important in NaCl fluids at temperature of 380 °C and density of 0.55 g/cm^3 (Driesner et al., 1998).

Our systematic *ab initio* calculations reveal a negative linear dependency of the degree of formation of the neutral species MCl_2Na(aq) with solution density. Charged complexes (e.g., $CuCl_2^-$ and $AuCl_2^-$) are predominant at high densities (>0.7 g/cm^3), even at high temperature, and neutral complexes are predominant at low densities (Fig. 6a and b). These simulations confirm the interpretation of *in situ* experimental XAS data accumulated in the last decade (e.g., Fulton et al., 2000a,b; Brugger et al., 2007; Liu et al., 2008), which emphasize the stability of the linear [$CuCl_2^-$] structure over a wide range of temperatures and pressures. In general, the majority of solubility data is also consistent with a predominance of $CuCl_2^-$ (e.g., Var'yash, 1992; Xiao et al., 1998; Liu et al., 2001). For low-density fluids, the available data also agree to the predominance of neutral species (Zajacz et al., 2011). Similarly for the Au(I)–chloride system, the MD results compare well to the available experimental data that suggest that $AuCl_2^-$ predominates in high-density fluids (e.g., Seward, 1973; Stefánsson and Seward, 2003; Pokrovski et al., 2009), while $NaAuCl_2$(aq) is predominant in low density supercritical fluids (Zajacz et al., 2010).

Our MD results have shown that the MD simulations are capable of revealing the loosely-bonded atoms in the outer coordination sphere of a complex, the key to understand the neutrality of the species in the high-temperature, low-density fluids. In contrast, *in situ* spectroscopic methods such as XAS failed to detect the second shell (Liu et al., 2008).

Because of the fast exchange of Na^+ in the $NaMCl_2$(aq) complexes, the ratio of $NaMCl_2$(aq) to MCl_2^- species is well constrained by the MD calculations. The linear relationship observed as a function of fluid density (Fig. 6a) further allows to extrapolate the MD results to different P,T conditions. We used these facts to calculate Gibbs free energies of reaction for the formation of the neutral complexes ($\Delta_r G^{\Theta}_{NaMCl_2(aq)}$). The reactions considered in our simulations of the Cu(I) system are as follows. Similar equations apply to the Au(I) system. The formations of the $NaCuCl_2$(aq) and $CuCl_2^-$ complexes can be written as:

$$Na^+ + Cu^+ + 2Cl^- = NaCuCl_2(aq) \quad (1)$$

$$Cu^+ + 2Cl^- = CuCl_2^- \quad (2)$$

The corresponding mass action equations are:

$$K_1 = \frac{\alpha_{NaCuCl_2(aq)}}{\alpha_{Cu^+}\cdot\alpha_{Na^+}\cdot\alpha^2_{Cl^-}} = \frac{[NaCuCl_2(aq)]\gamma_{NaCuCl_2(aq)}}{[Cu^+]\gamma_{Cu^+}\cdot\alpha_{Na^+}\cdot\alpha^2_{Cl^-}} \quad (3)$$

$$K_2 = \frac{\alpha_{CuCl_2^-}}{\alpha_{Cu^+}\cdot\alpha^2_{Cl^-}} = \frac{[CuCl_2^-]\gamma_{CuCl_2^-}}{\alpha_{Cu^+}\cdot\alpha^2_{Cl^-}} \quad (4)$$

where α_i and γ_i are the activity and activity coefficients of species i, respectively. The [] brackets represent concentrations of the bracketed species in molality. The activity of Na^+ (α_{Na^+}) and the activity coefficients $\gamma_{CuCl_2^-}$ and $\gamma_{NaCuCl_2(aq)}$ (Tables 4 and 5) were calculated based on the distribution of species calculations performed using the HCh software (Shvarov and Bastrakov, 1999).

We assume that

$$[NaCuCl_2(aq)] = N_{Na(Cu)}, \quad (5)$$

where $N_{Na(Cu)}$ values are obtained from the linear fitting results of the number of Na surrounding Cu retrieved by the MD simulations (Fig. 6). This assumption is reasonable: since $NaCuCl_2$(aq) and $CuCl_2^-$ are the only two Cu species in the solution, and there is only once Cu atom in the simulation box, the number of Na surrounding Cu represents the proportion of the Cu concentration as $NaCuCl_2$(aq), and $1 - N_{Na(Cu)}$ represents the concentration of $CuCl_2^-$. We note that the degree of association predicted from MD depends on the choice of the cutoff distance used to calculate $N_{Na(X)}$. For example, at 1000 °C, 1500 bar, $N_{Na(Cu)}$ decreases from 1.0 to 0.7 if the cutoff distance decreases from 4.5 to 4.0 Å, a range consistent with the geometric criterion used to define this cutoff distance (see Section 3.1). Importantly, the choice of the cutoff distance does not alter the trends shown in Fig. 6.

The Gibbs free energy of reaction (1) is:

$$\begin{aligned}\Delta_r G(1) &= \Delta_f G^{\Theta}_{NaCuCl_2(aq)} - \Delta_f G^{\Theta}_{Na^+} - \Delta_f G^{\Theta}_{Cu^+} - 2\Delta_f G^{\Theta}_{Cl^-} \\ &= -RT\ln K_1 \end{aligned} \quad (6)$$

Substituting α_{Cu^+} from Eq. (4) into Eq. (3), and making use of Eq. (5), we can rewrite Eq. (6) as:

$$\begin{aligned}&\Delta_f G^{\Theta}_{NaCuCl_2(aq)} - \Delta_f G^{\Theta}_{Na^+} - \Delta_f G^{\Theta}_{Cu^+} - 2\Delta_f G^{\Theta}_{Cl^-} \\ &= -RT\ln\frac{N_{Na(Cu)}\cdot K_2\cdot\gamma_{NaCuCl_2(aq)}}{(1-N_{Na(Cu)})\cdot\alpha_{Na^+}\cdot\gamma_{CuCl_2^-}}\end{aligned} \quad (7)$$

By rearranging Eq. (7) we obtain an expression for $\Delta_f G^{\Theta}_{NaCuCl_2(aq)}$:

$$\begin{aligned}\Delta_f G^{\Theta}_{NaCuCl_2(aq)} = &-RT\ln\frac{N_{Na(Cu)}\cdot K_2\cdot\gamma_{NaCuCl_2(aq)}}{(1-N_{Na(Cu)})\cdot\alpha_{Na^+}\cdot\gamma_{CuCl_2^-}} \\ &+ \Delta_f G^{\Theta}_{Na^+} + \Delta_f G^{\Theta}_{Cu^+} + 2\Delta_f G^{\Theta}_{Cl^-}\end{aligned} \quad (8)$$

The Gibbs free energies of formation from the elements $\Delta_f G^{\Theta}_{NaMCl_2(aq)}$ was retrieved using Gibbs free energy of formation (Eq. (1)) taken from Johnson et al. (1992) (Na^+), Liu and McPhail (2005) ($CuCl_2^-$), and Akinfiev and Zotov

Table 4
Estimation of the free energy of formation from the elements for $NaCuCl_2$(aq) from the MD simulations.

T (°C)	P (bar)	ρ (g/cm^3)	$N_{Na(Cu)}$ (Fit)*	log K_2[a]	$\gamma_{CuCl_2^-}$†	α_{Na^+}†	$\gamma_{NaCuCl_2(aq)}$†	$\Delta_f G^\Theta_{Na^+}$ (kJ/mol)††	$\Delta_f G^\Theta_{Cu^+}$ (kJ/mol)††	$\Delta_f G^\Theta_{Cl^-}$ (kJ/mol)††	$\Delta_f G^\Theta_{NaCuCl_2(aq)}$ (kJ/mol)†††	log K_p (MD)§	log K_p (HKF)§
25	1	1.18	0.09	5.45	0.64	1.66	0.90	−261.881	49.999	−131.290	−499.364	−1.09	−1.09
300	500	0.95	0.30	5.26	0.29	0.63	0.91	−282.685	33.370	−133.947	−578.551	0.33	0.35
300	1000	0.98	0.28	4.93	0.32	0.71	0.91	−282.870	32.699	−134.754	−575.748	0.18	0.15
300	2000	1.03	0.23	4.54	0.36	0.82	0.90	−282.854	31.884	−134.847	−570.050	−0.04	−0.04
500	600	0.67	0.56	8.33	0.02	0.02	0.91	−302.660	15.782	−92.788	−649.338	3.62	3.62
500	1000	0.76	0.48	6.37	0.11	0.17	0.91	−302.667	16.324	−117.712	−640.879	1.68	1.66
500	2000	0.87	0.38	5.17	0.22	0.42	0.91	−303.382	14.831	−128.309	−633.151	0.79	0.78
1000	2500	0.55	0.68	7.37	0.07	0.09	0.91	−364.249	−36.279	−78.206	−796.723	2.47	2.47
1000	5000	0.74	0.50	5.18	0.16	0.28	0.91	−368.465	−43.101	−107.367	−784.216	1.30	1.30

* $N_{Na(Cu)}$ is calculated from the linear fitting of $N_{Na(Cu)}$ as function of density for the data shown in Fig. 6c: $N_{Na(Cu)} = a + b * \rho$. The fitting considering the error bar gave $a = 1.191 \pm 0.20$; $b = -0.93 \pm 0.19$ with R^2 of 0.92.
[a] log K_2 of reaction $Cu^+ + 2Cl^- = CuCl_2^-$, as defined in Eq. (4); data from Liu and McPhail (1995).
† From HCh, speciation for a 1 molal CuCl and 3 molal NaCl solution.
†† Gibbs free energy of formation of Na^+ from Johnson et al. (1992); Cu^+ and Cl^- from Shock et al. (1997).
††† Gibbs free energy of formation of $NaCuCl_2$(aq) calculated following Eq. (8).
§ log K_p of reaction $Na^+ + CuCl_2^- = NaCuCl_2$(aq), from the MD results and from the HKF parameters listed in Table 6.

Table 5
Estimation of the free energy of formation from the elements for $NaAuCl_2$(aq) from the MD simulations.

T (°C)	P (bar)	ρ (g/cm^3)	$N_{Na(Au)}$ (Fit)*	log K_2[a]	$\gamma_{AuCl_2^-}$†	α_{Na^+}†	$\gamma_{NaAuCl_2(aq)}$†	$\Delta_f G^\Theta_{Na^+}$ (kJ/mol)††	$\Delta_f G^\Theta_{Au^+}$ (kJ/mol)††	$\Delta_f G^\Theta_{Cl^-}$ (kJ/mol)††	$\Delta_f G^\Theta_{NaAuCl_2(aq)}$ (kJ/mol)†††	log K_p (MD)§	log K_p (HKF)§
25	1	1.31	0.30	9.56	0.67	1.53	0.91	−261.881	163.176	−131.290	−413.413	−0.42	−0.42
300	500	1.05	0.45	6.34	0.32	0.60	0.91	−282.685	133.159	−133.947	−493.234	0.57	0.59
300	1000	1.09	0.42	6.02	0.35	0.68	0.91	−282.870	133.728	−134.754	−489.586	0.44	0.42
300	2000	1.14	0.40	5.64	0.39	0.78	0.91	−282.854	135.032	−134.847	−482.507	0.29	0.29
500	600	0.74	0.62	9.57	0.02	0.02	0.91	−302.660	110.316	−92.788	−572.370	3.57	3.57
500	1000	0.84	0.56	7.52	0.13	0.16	0.91	−302.667	110.031	−117.712	−565.234	1.75	1.74
500	2000	0.96	0.50	6.34	0.25	0.41	0.91	−303.382	110.749	−128.309	−557.026	0.94	0.95
1000	2500	0.61	0.69	9.86	0.09	0.09	0.91	−364.249	47.392	−78.206	−772.336	2.41	2.41
1000	5000	0.82	0.58	7.81	0.19	0.28	0.91	−368.465	48.100	−107.367	−758.951	1.38	1.38

* $N_{Na(Au)}$ (Fit) is calculated from the linear fitting of $N_{Na(Au)}$ as function of density: $N_{Na(Au)} = a + b * \rho$. The fitting considering the error bar gave $a = 1.04 \pm 0.36$; $b = -0.57 \pm 0.47$ with R^2 of 0.84.
[a] log K_2 of reaction $Au^+ + 2Cl^- = AuCl_2^-$; data from Akinfiev and Zotov (2001).
† From HCh, speciation for a 1 molal AuCl and 3 molal NaCl solution.
†† Gibbs free energy of formation of Na^+ from Johnson et al. (1992); Au^+ and Cl^- from Shock et al. (1997).
††† Gibbs free energy of formation of $NaAuCl_2$(aq) calculated in a manner similar as for Cu^+, following Eq. (8).
§ log K_p of reaction $Na^+ + AuCl_2^- = NaAuCl_2$(aq), from the MD results and from the HKF parameters listed in Table 6.

(2001) ($AuCl_2^-$). The values used for calculating $\Delta_f G^\Theta_{NaCuCl_2(aq)}$ are given in Table 4. A similar approach was used to calculate $\Delta_f G^\Theta_{NaAuCl_2(aq)}$, with parameters provides in Table 5. These $\Delta_f G^\Theta_{NaAuCl_2(aq)}$ values were used to regress Helgeson–Kirkham–Flowers (HKF) equation of state parameters (Tanger and Helgeson, 1988) using the OptimB software (Shvarov, 1993). These HKF parameters are listed in Table 6, and can be used to estimate the degree of association in high density ($\geqslant$0.4 g/cm^3) fluids up to 1000 °C, 5 kbar. LogK of forming neutral complexes $NaCuCl_2$ and $NaAuCl_2$ as functions of temperature at selected pressure is plotted using fitted HKF parameters (Fig. 9).

It should be noted that this approach reproduces the ion associations predicted from the MD results within the HCh thermodynamic framework. The thermodynamic properties derived (Tables 4 and 5) from our simulation results represent the first approximation for these properties. We assume that a single metal ion and 55 waters in the periodic simulation box can represents a 1 molal metal concentra-

Table 6
Equation-of-state parameters and standard partial molal properties (HKF parameters) for the $NaCuCl_2$(aq) and $NaAuCl_2$(aq) complexes regressed from the MD results.

Parameters	$NaCuCl_2$(aq)	$NaAuCl_2$(aq)
$\Delta_f \bar{G}^0_{P_r,T_r}$ (Cal mol^{-1})	−119 351	−98 808
$\bar{S}^0_{P_r,T_r}$ (Cal mol^{-1} K^{-1})	71.677	66.537
a_1 (Cal mol^{-1} bar^{-1}) × 10	−1.3092	−0.1304
a_2 (Cal mol^{-1}) × 10^{-2}	49.0356	53.4503
a_3 (Cal mol^{-1} bar^{-1})	60.7152	109.7903
a_4 (Cal mol^{-1}) × 10^{-4}	−4.8061	−4.9886
c_1 (Cal mol^{-1})	5.2670	35.5655
c_2 (Cal K mol^{-1}) × 10^{-4}	−9.3425	−26.6574
ω_{P_r,T_r}(Cal mol^{-1}) × 10^{-5}	−0.1693	−0.1177

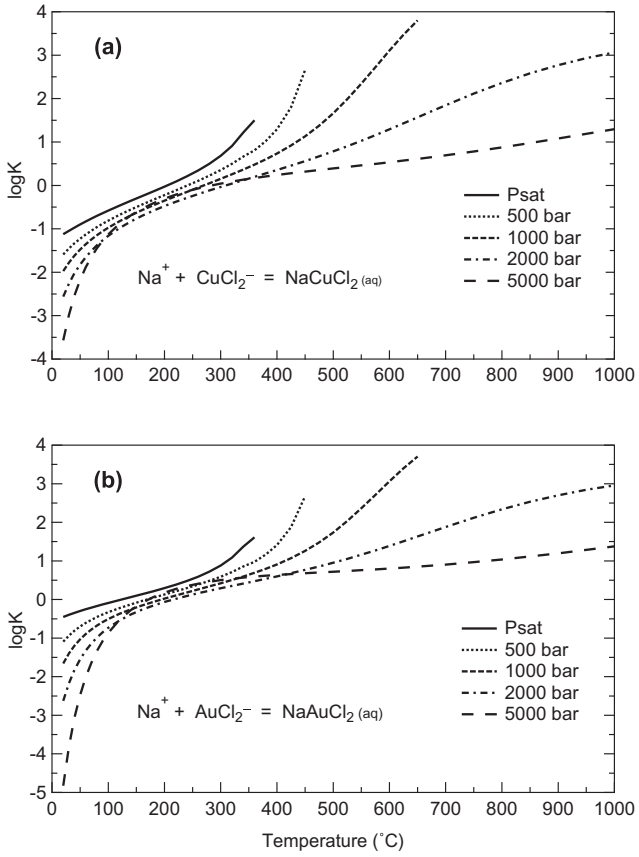

Fig. 9. LogK of forming neutral complexes $NaCuCl_2$ and $NaAuCl_2$ as functions of temperature using the HKF parameters fitted in Table 6.

tion *in infinite dilution of the metal ion* (i.e., neglecting Cu–Cu or Au–Au interactions). The main uncertainty is related to the uncertainty in $N_{Na(Cu/Au)}$ (Tables 4 and 5), related to the limited length of the MD simulations and to systematic errors in $N_{Na(Cu/Au)}$ induced by the choice of the cutoff distance. We estimate the uncertainty in the predicted ion associations to be ~20%.

4.3. Density dependence of hydration of ions and metal complexes

The number of water molecules (i.e., the hydration number) surrounding Cu^+, Au^+, Na^+ and Cl^- ions decreases linearly when fluid density decreases (Fig. 6c and d). The decrease of hydration number with the decrease of density has been demonstrated in previous experimental (Archibald et al., 2001, 2002) and theoretical studies (e.g., Hemley et al., 1992; Driesner et al., 1998; Seward and Driesner, 2004; Sherman, 2007). Note that in contrast to the density dependence of the hydration number, the Na–O and Cl–O distances change with temperature rather than density (see Section 3.3). The decrease of Na–O distances with increasing temperature may result from the faster kinetics at high temperature increasing the attractive force of Na^+ and negative charged oxygen in H_2O (recognized as O^{2-} ions). Similarly, the increasing kinetics at high temperature increases the repulsive force of Cl^- and O^{2-} ionic pairs, which lead to the increase of Cl–O distances.

There are numerous experimental studies on the solubility of NaCl(s) and hydration of NaCl ion pairs in water vapor (see review of Palmer et al., 2004). In these studies, a linear trend was established between the solubility of NaCl(s) and the density of the water, with the intersection of Y axis as concentration constants, and the slope being interpreted as hydration numbers (e.g., Armellini and Tester, 1993; Palmer et al., 2004):

$$C_{NaCl} = \log K_c + nH_2O \log \rho, \quad (9)$$

where C_{NaCl} is the concentration of NaCl in the fluid, n is the number of hydration water and ρ is the density of water. Eq. (9) is valid for an ideal gas. This approach has been used to interpret the solubility of Ag(I) and Cu(I) in subcritical water vapor (Migdisov et al., 1999; Archibald et al., 2002; Williams-Jones et al., 2002) and in supercritical water near the critical isochore (Liu et al., 2008). Eq. (9) implies that the hydration number is independent of density at a given temperature. Our results and other MD studies (Driesner et al., 1998; Lee et al., 1998; see reviews in Seward and Driesner, 2004) all suggest that hydration numbers should decrease with fluid density, and therefore the hydration number implied from the regression of experimental salt solubility (Eq. (9)) is not accurate at a given temperature, although it may indicate a first-order estimation. Our MD results suggest that the hydration number of the $[H_2O–Cu–Cl](aq)$ complex decreases from ~7 at 420 bar to ~4.3 at 290 bar (400 °C; Fig. 7), while the experimental

data of Liu et al. (2008) suggest a constant hydration at ~1.8. In contrast, Archibald et al. (2001) describe a decrease in hydration number for [H_2O–Au–Cl](aq) from 5 at 300 °C to 3 at 360 °C; in this case the MD predictions (hydration number of 3 at 340 °C; Fig. 8) correspond to the interpretation of Archibald et al. (2001).

4.4. Translational entropy and the density dependence of hydrothermal reactions

It is well documented that the free energies of reactions involving aqueous complexes often vary in a linear fashion with water density (as related to pressure) at fixed temperature (Anderson et al., 1991; Manning, 1998; Dolejš and Manning, 2010; Dolejš, 2013). Our MD data provide a simple explanation for this empirical observation, by revealing a linear correlation (i.e., hydration number $\sim a + b\rho_s$) between the solution density and the hydration number of Cu(I) and Au(I) complexes that show no evidence for significant change in stoichiometry and geometry over the investigated P, T range. Consequently, the empirical correlation between Log K and water density can be explained by assuming that the change in translational entropy is proportional to the change in hydration number:

$$\begin{aligned}\Delta_r G = \Delta_r H - T\Delta_r S = \Delta_r H - T(a + b\rho_s) = -RT\ln K\\ \text{so}: \ln K = \frac{\Delta_r H - Ta + Tb\rho}{RT}\\ \sim \rho \ @ \text{ constant } T\end{aligned} \quad (10)$$

Since the hydration numbers of Na and Cl decline with the decrease of density (increase of volume), the Cl/Na hydrated ions may have smaller volume at high density, and the volume would increase upon release of the hydration waters to solution, e.g.,

$$V_{Cl(H_2O)_n}(\text{high density}) < V_{Cl(H_2O)_{n-m}} + mH_2O(\text{low density}) \quad (11)$$

Indeed, translational entropy can also explain the formation of neutral ion pairs rather than charged complexes such as $CuCl_2^-$ in low density supercritical fluids. Assuming that the largest contribution of hydration to the translational entropy is related to the more strongly bonded and ordered first shell hydration, we can write:

$$CuNaCl_2(aq) + mH_2O \rightarrow CuCl_2^- + Na\cdot(H_2O)_m^+ \quad (12)$$

At high density, Na^+ attracts more water to form hydration ions ($m \geqslant 4$ when density $\geqslant 0.8$), so the preferred reaction direction is to form the charged complexes $CuCl_2^-$. At low density, the hydration water of Na ions is released ($m \leqslant 3$ when density $\leqslant 0.5$ g/cm^3), so the preferred reaction direction is to form neutral complex $CuNaCl_2$(aq). The translational entropy of the left side in Eq. (12) is higher than the right side because there are more free species (more translational degrees of freedom).

Archibald et al. (2001, 2002) suggested that the solubilities of Au and Cu decreased with increasing temperature as a result of decreasing hydration number, which is consistent with the results from our MD simulations. In fluids with low chloride concentrations, the less hydrated Cl^- ions (i.e., hydration of 0.7 at fluid density of 0.1 g/cm^3; No. 4 in Table 3 and Fig. 8d) at lower density may affect metal solubility. In low-density chloride-rich fluids, Zajacz et al. (2010) noticed that at a constant Cl (NaCl + HCl) concentration of 0.75 m, gold solubility increased with the increasing of NaCl/(NaCl + HCl) ratio to 0.5, and then decreased with higher ratio of NaCl. As indicated by our MD simulations, this dependence of Au solubility on NaCl/(NaCl + HCl) can be explained by the competition between the formation of $AuNaCl_2$ and NaCl (aq) species.

The traditional Born-model description explains the increase in ion association with decreasing solution density as resulting from the decrease in dielectric constant of the solvent (Born, 1920; Seward and Barnes, 1997). A molecular description, however, explains the ion association as resulting from the increase in translational entropy of products relative to the reactants. The translation entropy of the products is greater than that of the reactants since the hydration waters surrounding Na^+ are liberated and there are now more translational degrees of freedom. Because of the increase in translational entropy, the ion association is favored by temperature. Moreover, the entropy of liberated water molecules will increase with decreasing fluid density; consequently, the ion association is favored by decreasing fluid density.

ACKNOWLEDGEMENT

Research funding was provided by the Australian Research Council (ARC) to J.B. (DP0878903), the Minerals Down Under Flagship to W.L. and NERC Grant NE/I02349X/1 – Transport of Lithophile Elements in Magmatic-Hydrothermal Fluids to D.M.S. The MD calculations were supported by iVEC through the use of advanced computing resources located in Perth, Australia, and the computational facilities of the Advanced Computing Research Centre in University of Bristol, UK. This paper is part of Yuan Mei's Ph.D. thesis. Y.M. acknowledges the University of Adelaide for IPRS scholarship and CSIRO Minerals Down Under Flagship for a scholarship top-up. We are grateful to Dr. Zoltan Zajacz and two anonymous reviewers for their helpful comments on this manuscript.

APPENDIX A. SUPPLEMENTARY DATA

Supplementary data associated with this article can be found, in the online version, at http://dx.doi.org/10.1016/j.gca.2014.01.033.

REFERENCES

Akinfiev N. N. and Zotov A. V. (2001) Thermodynamic description of chloride, hydrosulfide, and hydroxo complexes of Ag(I), Cu(I), and Au(I) at temperatures of 25–500 °C and pressures of 1–2000 bar. *Geochem. Int.* **39**, 990–1006.

Anderson G. M., Castet S., Schott J. and Mesmer R. E. (1991) The density model for estimation of thermodynamic parameters of reactions at high temperatures and pressures. *Geochim. Cosmochim. Acta* **55**, 1769–1779.

Archibald S. M., Migdisov A. A. and Williams-Jones A. E. (2001) The stability of Au–chloride complexes in water vapor at elevated temperatures and pressures. *Geochim. Cosmochim. Acta* **65**, 4413–4423.

Archibald S. M., Migdisov A. A. and Williams-Jones A. E. (2002) An experimental study of the stability of copper chloride complexes in water vapor at elevated temperatures and pressures. *Geochim. Cosmochim. Acta* **66**, 1611–1619.

Armellini F. J. and Tester J. W. (1993) Solubility of sodium chloride and sulfate in sub-and supercritical water vapor from 450–550 °C and 100–250 bar. *Fluid Phase Equilib.* **84**, 123–142.

Barnes H. L. (1997) *Geochemistry of Hydrothermal Ore Deposits*. Wiley, New York, 795 pp.

Born M. (1920) Volumen und Hydratationswärme der Ionen. *Zeitschrift für Physik* **1**, 45–48.

Brugger J., Etschmann B., Liu W., Testemale D., Hazemann J. L., Emerich H., van Beek W. and Proux O. (2007) An XAS study of the structure and thermodynamics of Cu(I) chloride complexes in brines up to high temperature (400 °C, 600 bar). *Geochim. Cosmochim. Acta* **71**, 4920–4941.

Brugger J., Pring A., Reith F., Ryan C., Etschmann B., Liu W. H., O'Neill B. and Ngothai Y. (2010) Probing ore deposits formation: new insights and challenges from synchrotron and neutron studies. *Radiat. Phys. Chem.* **79**, 151–161.

Burgess J. (1978) *Metal Ions in Solution*. Ellis Horwood Ltd., Chichester, distributed by John Wiley and Sons, Chichester and New York, 481 pp.

Car R. and Parrinello M. (1985) Unified approach for molecular dynamics and density-functional theory. *Phys. Rev. Lett.* **55**, 2471–2474.

Cossi M., Barone V., Cammi R. and Tomasi J. (1996) *Ab initio* study of solvated molecules: a new implementation of the polarizable continuum model. *Chem. Phys. Lett.* **255**, 327–335.

Dolejš D. (2013) Thermodynamics of aqueous species at high temperatures and pressures: equations of state and transport theory. *Rev. Mineral. Geochem.* **76**, 35–79.

Dolejš D. and Manning C. E. (2010) Thermodynamic model for mineral solubility in aqueous fluids: theory, calibration and application to model fluid-flow systems. *Geofluids* **10**, 20–40.

Driesner T. (2007) The system H_2O–NaCl. Part II: correlations for molar volume, enthalpy, and isobaric heat capacity from 0 to 1000°C, 1 to 5000bar, and 0 to 1 XNaCl. *Geochim. Cosmochim. Acta* **71**, 4902–4919.

Driesner T. and Heinrich C. A. (2007) The system H_2O–NaCl. Part I: correlation formulae for phase relations in temperature–pressure–composition space from 0 to 1000°C, 0 to 5000bar, and 0 to 1 XNaCl. *Geochim. Cosmochim. Acta* **71**, 4880–4901.

Driesner T., Seward T. M. and Tironi I. G. (1998) Molecular dynamics simulation study of ionic hydration and ion association in dilute and 1 molal aqueous sodium chloride solutions from ambient to supercritical conditions. *Geochim. Cosmochim. Acta* **62**, 3095–3107.

Etschmann B. E., Liu W., Testemale D., Müller H., Rae N. A., Proux O., Hazemann J. L. and Brugger J. (2010) An in situ XAS study of copper(I) transport as hydrosulfide complexes in hydrothermal solutions (25–592 °C, 180–600 bar): speciation and solubility in vapor and liquid phases. *Geochim. Cosmochim. Acta* **74**, 4723–4739.

Frank M. R., Simon A. C., Pettke T., Candela P. A. and Piccoli P. M. (2011) Gold and copper partitioning in magmatic-hydrothermal systems at 800 °C and 100 MPa. *Geochim. Cosmochim. Acta* **75**, 2470–2482.

Fulton J. L., Hoffmann M. M. and Darab J. G. (2000a) An X-ray absorption fine structure study of copper(I) chloride coordination structure in water up to 325 °C. *Chem. Phys. Lett.* **330**, 300–308.

Fulton J. L., Hoffmann M. M., Darab J. G., Palmer B. J. and Stern E. A. (2000b) Copper(I) and copper(II) coordination structure under hydrothermal conditions at 325 °C: an X-ray absorption fine structure and molecular dynamics study. *J. Phys. Chem., A* **104**, 11651–11663.

Harris D. J., Brodholt J. P. and Sherman D. M. (2003) Zinc complexation in hydrothermal chloride brines: results from ab initio molecular dynamics calculations. *J. Phys. Chem. A* **107**, 1050–1054.

Hemley J., Cygan G., Fein J., Robinson G. and d'Angelo W. (1992) Hydrothermal ore-forming processes in the light of studies in rock-buffered systems; I, iron–copper–zinc–lead sulfide solubility relations. *Econ. Geol.* **87**, 1–22.

Humphrey W., Dalke A. and Schulten K. (1996) VMD: visual molecular dynamics. *J. Mol. Graph.* **14**, 33–38.

Johnson J. W., Oelkers E. H. and Helgeson H. C. (1992) SUPCRT92: a software package for calculating the standard molal thermodynamic properties of minerals, gases, aqueous species, and reactions from 1 to 5000 bar and 0–1000 °C. *Computers Geosci.* **18**, 899–947.

Laasonen K., Pasquarello A., Car R., Lee C. and Vanderbilt D. (1993) Car-Parrinello molecular dynamics with Vanderbilt ultrasoft pseudopotentials. *Phys. Rev. B* **47**, 10142–10153.

Lee S., Cummings P., Simonson J. and Mesmer R. (1998) Molecular dynamics simulation of the limiting conductance of NaCl in supercritical water. *Chem. Phys. Lett.* **293**, 289–294.

Lerchbaumer L. and Audétat A. (2012) High Cu concentrations in vapor-type fluid inclusions: an artifact? *Geochim. Cosmochim. Acta* **88**, 255–274.

Liu W. and McPhail D. C. (2005) Thermodynamic properties of copper chloride complexes and copper transport in magmatic-hydrothermal solutions. *Chem. Geol.* **221**, 21–39.

Liu W., McPhail D. C. and Brugger J. (2001) An experimental study of copper(I)-chloride and copper(I)-acetate complexing in hydrothermal solutions between 50 and 250 °C and vapor-saturated pressure. *Geochim. Cosmochim. Acta* **65**, 2937–2948.

Liu W., Brugger J., Etschmann B., Testemale D. and Hazemann J.-L. (2008) The solubility of nantokite (CuCl(s)) and Cu speciation in low-density fluids near the critical isochore: an in-situ XAS study. *Geochim. Cosmochim. Acta* **72**, 4094–4106.

Liu X., Lu X., Wang R., Zhou H. and Xu S. (2011) Speciation of gold in hydrosulphide-rich ore-forming fluids: insights from first-principles molecular dynamics simulations. *Geochim. Cosmochim. Acta* **75**, 185–194.

Liu X., Lu X., Wang R. and Zhou H. (2012) Silver speciation in chloride-containing hydrothermal solutions from first principles molecular dynamics simulations. *Chem. Geol.* **294–295**, 103–112.

Manning C. E. (1998) Fluid composition at the blueschist – eclogite transition in the model system Na_2O–MgO–Al_2O_3–SiO_2–H_2O–HCl. *Schweiz. Mineral. Petrogr. Mitt.* **78**, 225–242.

Mei Y., Sherman D. M., Liu W. and Brugger J. (2013a) Ab initio molecular dynamics simulation and free energy exploration of copper(I) complexation by chloride and bisulfide in hydrothermal fluids. *Geochim. Cosmochim. Acta* **102**, 45–64.

Mei Y., Sherman D. M., Liu W. and Brugger J. (2013b) Complexation of gold in S_3^--rich hydrothermal fluids: evidence from ab-initio molecular dynamics simulations. *Chem. Geol.* **347**, 34–42.

Migdisov A. A., Williams-Jones A. and Suleimenov O. (1999) Solubility of chlorargyrite (AgCl) in water vapor at elevated temperatures and pressures. *Geochim. Cosmochim. Acta* **63**, 3817–3827.

Palmer D. A., Simonson J. and Jensen J. (2004) *Partitioning of Electrolytes to Steam and their Solubilities in Steam. Aqueous Systems at Elevated Temperatures and Pressures*. Elsevier, New York, 409–439.

Perdew J. P., Burke K. and Ernzerhof M. (1996) Generalized gradient approximation made simple. *Phys. Rev. Lett.* **77**, 3865–3868.

Pokrovski G. S., Roux J. and Harrichoury J. C. (2005) Fluid density control on vapor-liquid partitioning of metals in hydrothermal systems. *Geology* **33**, 657–660.

Pokrovski G. S., Tagirov B. R., Schott J., Bazarkina E. F., Hazemann J.-L. and Proux O. (2009) An in situ X-ray absorption spectroscopy study of gold-chloride complexing in hydrothermal fluids. *Chem. Geol.* **259**, 17–29.

Pokrovski G. S., Roux J., Ferlat G., Jonchiere R., Seitsonen A. P., Vuilleumier R. and Hazemann J.-L. (2013) Silver in geological fluids from in situ X-ray absorption spectroscopy and first-principles molecular dynamics. *Geochim. Cosmochim. Acta* **106**, 501–523.

Rempel K. U., Liebscher A., Meixner A., Romer R. L. and Heinrich W. (2012) An experimental study of the elemental and isotopic fractionation of copper between aqueous vapour and liquid to 450 °C and 400 bar in the CuCl–NaCl–H_2O and CuCl–NaHS–NaCl–H_2O systems. *Geochim. Cosmochim. Acta* **94**, 199–216.

Seward T. M. (1973) Thio complexes of gold and the transport of gold in hydrothermal ore solutions. *Geochim. Cosmochim. Acta* **37**, 379–399.

Seward T. M. and Barnes H. L. (1997) Metal transport by hydrothermal ore fluids. In *Geochemistry of Hydrothermal Ore Deposits* (ed. H. L. Barnes). Wiley, New York.

Seward T. and Driesner T. (2004) Hydrothermal solution structure: experiments and computer simulations. In *Aqueous Systems at Elevated Temperatures and Pressures* (eds. D. A. Palmer, R. Fernández-Prini and A. H. Havey). Elsevier.

Sharps J. A., Brown, Jr, G. E. and Stebbins J. F. (1993) Kinetics and mechanism of ligand exchange of Au(III), Zn(II), and Cd(II) chlorides in aqueous solution: an NMR study from 28–98°C. *Geochim. Cosmochim. Acta* **57**, 721–731.

Shock E. L., Sassani D. C., Willis M. and Sverjensky D. A. (1997) Inorganic species in geologic fluids - correlations among standard molal thermodynamic properties of aqueous ions and hydroxide complexes. *Geochim. Cosmochim. Acta* **61**, 907–950.

Shvarov Y. V. (1993) *UT-HEL: IBM Computer Code for Calculating the HKF revised Equation of State Parameters for Aqueous Species*. Moscow State University.

Shvarov Y. and Bastrakov E. (1999) *HCh: A Software Package for Geochemical Modelling*. User's guide. AGSO, record 1999/25, 60 pp.

Sherman D. M. (2007) Complexation of Cu+ in hydrothermal NaCl brines: ab initio molecular dynamics and energetics. *Geochim. Cosmochim. Acta* **71**, 714–722.

Sherman D. M. and Collings M. D. (2002) Ion association in concentrated NaCl brines from ambient to supercritical conditions: results from classical molecular dynamics simulations. *Geochem. Trans.* **3**, 102–107.

Simon A. C., Frank M. R., Pettke T., Candela P. A., Piccoli P. M. and Heinrich C. A. (2005) Gold partitioning in melt–vapor–brine systems. *Geochim. Cosmochim. Acta* **69**, 3321–3335.

Simon A. C., Pettke T., Candela P. A., Piccolli P. M. and Heinrich C. A. (2006) Copper partitioning in a melt–vapor–brine–magnetite–pyrrhotite assemblage. *Geochim. Cosmochim. Acta* **70**, 5583–5600.

Stefánsson A. and Seward T. M. (2003) Stability of chlorido gold(I) complexes in aqueous solutions from 300 to 600 °C and from 500 to 1800 bar. *Geochim. Cosmochim. Acta* **67**, 4559–4576.

Tanger J. C. I. and Helgeson H. C. (1988) Calculation of the thermodynamic and transport properties of aqueous species at high pressures and temperatures: revised equations of state for the standard partial molal properties of ions and electrolytes. *Am. J. Sci.* **288**, 19–98.

Var'yash L. N. (1992) Cu(I) complexing in NaCl solutions at 300 and 350 °C. *Geochem. Int.* **29**, 84–92.

Williams-Jones A. E., Migdisov A. A., Archibald S. M. and Xiao Z. (2002) Vapor-transport of ore metals. *Water–Rock Interact.* **7**, 279–305.

Xiao Z., Gammons C. H. and Williams-Jones A. E. (1998) Experimental study of copper(I) chloride complexing in hydrothermal solutions at 40–300 °C and saturated water vapor pressure. *Geochim. Cosmochim. Acta* **62**, 2949–2964.

Zajacz Z., Seo J. H., Candela P. A., Piccoli P. M., Heinrich C. A. and Guillong M. (2010) Alkali metals control the release of gold from volatile-rich magmas. *Earth Planet. Sci. Lett.* **297**, 50–56.

Zajacz Z., Seo J. H., Candela P. A., Piccoli P. M. and Tossell J. A. (2011) The solubility of copper in high-temperature magmatic vapors: a quest for the significance of various chloride and sulfide complexes. *Geochim. Cosmochim. Acta* **75**, 2811–2827.

Zezin D. Y., Migdisov A. A. and Williams-Jones A. E. (2007) The solubility of gold in hydrogen sulfide gas: an experimental study. *Geochim. Cosmochim. Acta* **71**, 3070–3081.

Zezin D. Y., Migdisov A. A. and Williams-Jones A. E. (2011) The solubility of gold in H_2O–H_2S vapour at elevated temperature and pressure. *Geochim. Cosmochim. Acta* **75**, 5140–5153.

Associate editor: Jun-ichiro Ishibashi